Final Report

Regional Ecosystem-Atmosphere CO_2 Exchange via Atmospheric Budgets

A Collaborative Effort between
A. Scott Denning, Colorado State University
Kenneth Davis, Pennsylvania State University

DOE-FG02-02ER63474/5

Program Manager: Roger C. Dahlman

Background

The atmospheric burden of CO_2 is steadily increasing in response to widespread anthropogenic combustion of fossil fuels, approximately 7 PgC yr^{-1} of emissions to the atmosphere. A large portion of this carbon, about 4 PgC yr^{-1}, is absorbed by the earth's oceans and terrestrial ecosystems. This uptake varies annually from 1 to 6 PgC yr^{-1} (Conway et al, 1994). Approximately one-half of this large and variable sink is believed to be due to net uptake by terrestrial ecosystems (Ciais et al, 1995; Battle et al, 2000). Understanding the causes and documenting the spatial distribution of this terrestrial sink of carbon are primary goals of carbon cycle science. Another primary need is to understand the cause of the large interannual variability in the terrestrial carbon sink. Such understanding would enable us to better predict the future response of the carbon cycle to climate and land use change, and may suggest ways to mitigate climate change via management of the terrestrial carbon cycle. Progress is hampered by our limited ability to quantify the terrestrial carbon cycle on appropriate spatial and temporal scales. Measurements of ecosystem-atmosphere CO_2 exchange that integrate over domains of similar ecosystem and climate, and across seasons will greatly extend our understanding of the terrestrial carbon cycle.

This collaborative project has supported ongoing work to develop and understand analyses of highly calibrated CO_2 mixing ratio measurements on communications towers in northern Wisconsin (the Ring of Towers, 2003 and 2004 data collection), and on several AmeriFlux towers. At Penn State, it has additionally supported substantial instrument development to improve the precision of the sensors deployed long-term to AmeriFlux sites.

Observations

As a first step towards implementing atmospheric budget or inversion methodology on a regional scale, a network of five relatively inexpensive CO_2 mixing ratio measurement systems were deployed on towers in northern Wisconsin between April and August 2004. Four systems were distributed on a circle of roughly 150-km radius, surrounding one centrally located system at the WLEF tower in Park Falls, WI. Additional data from the Sylvania, MI, AmeriFlux tower was incorporated into the dataset. The five systems used LiCor-820 infrared CO_2 analyzers and were calibrated every two hours using four samples

known to within ± 0.2 ppm CO_2. Frequent calibration is necessary to characterize and remove the nonlinear response of the CO_2 sensor to changes in temperature and pressure. Before deploying the five CO_2 systems, their relative accuracy was tested by sampling air in parallel from a four-liter sample volume with a fan actively circulating the air. For the tests, each system used its own set of calibration standards to measure the relative accuracy in the field. The relative agreement between all systems was better than ± 0.3 ppm, which may include small errors in the field standards. A LI-7000 connected in series with one of the five systems revealed no systematic bias associated with the use of the LI-820.

As a further means to evaluate the accuracy of the systems, one system was deployed at the WLEF tower in Park Falls, WI, (Bakwin et al., 1998) where a NOAA-ESRL system also measured CO_2 mixing ratio. The PSU system sample line branched off from the NOAA-ESRL system 76-m sample line at the base of the tower to ensure that both systems were sampling identical air. The NOAA-ESRL and PSU systems had independent filtering and, more importantly, independent drying. In addition, the NOAA-ESRL system used a LI-6251. The difference between the CO_2 mixing ratio measured by the two systems for the times in which both systems were operational is

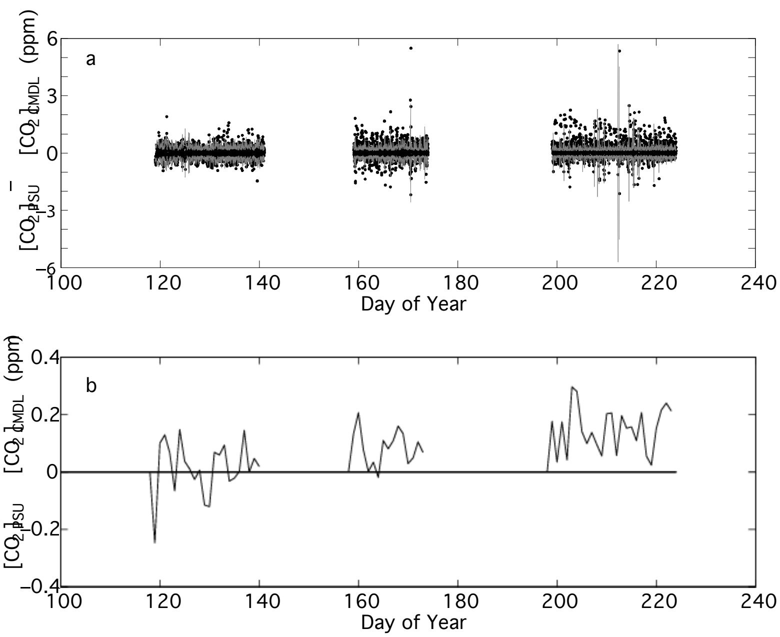

Figure 1. Difference between the CO_2 mixing ratio measured by the PSU and NOAA-ESRL systems at the WLEF tower (76-m level) during April–August 2004. **a)** 12-min data (solid circles) and uncertainty estimate of the NOAA-ESRL system (gray line), and **b)** difference between the daily average [CO_2] measurements.

shown in Fig. 1a.

The estimated uncertainty of the NOAA-ESRL system, calculated such that the actual value should be within one times the uncertainty estimate of the measured value 67% of the time, is also shown (A. Andrews, personal communication). The PSU estimate of the CO_2 mixing ratio is within one times the uncertainty estimate of the NOAA-ESRL value for 57% of the observations; the average ESRL uncertainty estimate is 0.29 ppm. The PSU value is within 0.5 ppm of the NOAA-ESRL value for 83% of the values, and 96% of the PSU values are within 1 ppm of the NOAA-ESRL values. The daytime-only percentages are similar. The difference between the daily mean PSU value and the daily mean NOAA-ESRL value (Fig. 2b) is consistently less than ±0.3 ppm.

To show the utility of such a regional scale network in determining the spatially- and temporally-varying regional flux, we calculate, in the simplest possible manner, the Lagrangian estimate of the daytime CO_2 flux on two days in which the wind direction was such that parcels traveled across the study domain and in which the wind speed was relatively constant for several hours. The days chosen for the analysis (19−20 June 2004) had simple CO_2 signals, with no evidence of frontal passages or pollution events. The parcel transit times between upwind and downwind sites were about 6 – 8 hr for 19 June and 3 hr for 20 June. The change in CO_2 mixing ratio of parcels traveling between sites is at least 2.6 ppm, which is large compared to the accuracy of the systems, and typical of the horizontal gradients we might expect over a distance of 100-200 km under fair weather conditions. Using an estimate of the boundary layer depth based on temperature soundings and measured heat fluxes, and assuming the entrainment flux to be zero, the estimated flux is −10 to −11 µmol m^2 s^{-1} on June 19 and −18 to −19 µmol m^2 s^{-1} on June 20. We estimate the uncertainty of the flux, based on errors in the BL depth, transit times, and [CO2], to be at least 3 µmol m^2 s^{-1}. For comparison, the midday average net ecosystem-atmosphere exchange (NEE) measured at 30 m on the WLEF tower is −9 µmol m^2 s^{-1} on both 19 and 20 June. While the 122-m and 396-m data are generally used to calculate the flux on unstable days such as these, the data at those heights are, unfortunately, not available. A typical value for the difference between the flux measured at 30 m and the higher levels is −5 µmol m^2 s^{-1}; thus the actual NEE is likely closer to −14 µmol m^2 s^{-1}. This rough estimate shows that the Ring CO_2 measurements should yield very reasonable results when interpreted in a full inversion scheme.

As another example of the data captured with a regional scale network, we show data during a frontal passage. Within the regional network on 29 April 2004, all six sites (with the possible exception of Wittenberg) show an abrupt increase in CO_2 mixing ratio followed by a gradual decline (Fig. 2). The timing of the increase in CO_2 mixing ratio coincides with a frontal passage through the region, from the northwest to the southeast. Prior to the frontal passage the CO_2 mixing ratio measured at 76 m at WLEF decreased from 386 ppm at 0230 GMT to 377 ppm at

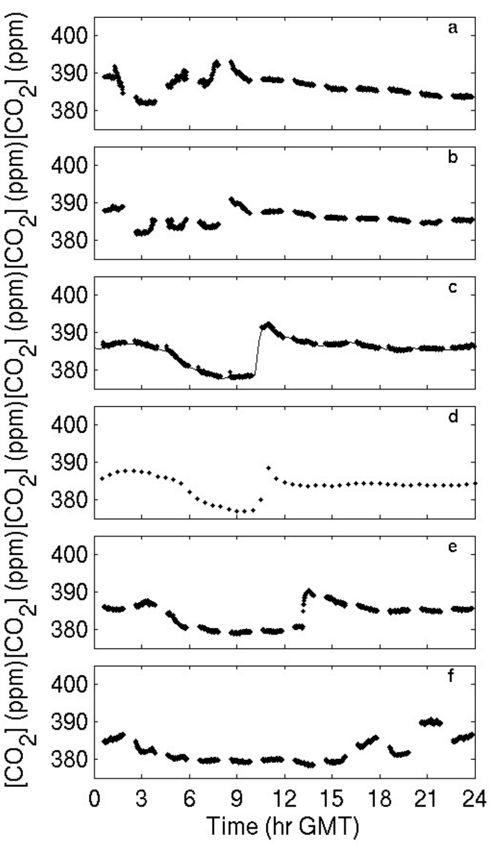

Figure 2. CO_2 mixing ratio measured at five sites within the regional network for 29 April 2004, a) Buhl, b) Bayfield, c) WLEF, d) Sylvania, e) Fence, and f) Wittenberg. All measurement heights are 76 m and data shown are 1-min averages, with the exception of Sylvania where the measurement height is 36 m and the data are available every 30 min. Both a PSU system (dots) and a NOAA-ESRL system (line) recorded data at the WLEF tower. The approximate times of frontal passage at each site (to the nearest hour) as determined from surface observations of pressure, temperature, and winds are a) 0600, b) 0900, c) 1000, d) 1000, e) 1300, f) 1300 GMT. Sunset at WLEF occurred at 0106 GMT, and sunrise at 1051 GMT.

0830 GMT (Fig. 2c). The frontal passage occurred during a calibration cycle of the PSU system so no data were recorded during the rapid change, but the CO_2 mixing ratio immediately before the frontal passage was 379 ppm and immediately after was 391 ppm. The ESRL system recorded two intermediate points between the prefrontal value and the postfrontal value 36 min later. After the frontal passage, the CO_2 mixing ratio then gradually fell to 386 ppm and remained relatively constant for the duration of the day. While the frontal case is not easily interpreted in terms of local biological fluxes, it clearly illustrates that the mixing ratio measurements on small towers capture coherent regional changes in CO_2.

Numerical tools

This project had made use of a comprehensive suite of numerical models and analysis tools for the study of the continental carbon cycle. These tools have been developed and tested by the investigators over the past 15 years, partly with support from DOE. They include:

- The **Simple Biosphere model (SiB)**, which represents ecosystem physiology, including photosynthesis, respiration, and decomposition on local, regional, and global scales;
- The **Regional Atmospheric Modeling System (RAMS)**, which simulates weather, winds, and atmospheric tracer transport as well as land-atmosphere interaction. The coupled SiB-RAMS model has been used to simulate gridded NEE and atmospheric CO_2 from the scale of large PBL eddies to the entire continent on a set of telescoping two-way nested grids;
- The CSU **Lagrangian Particle Dispersion Model (LPDM)**, which calculates backward-in-time trajectories to relate observed changes in CO_2 mixing ratio to surface fluxes upstream;

LPDM and Formulation of NEE and Mixing Ratio Variations

We have developed a method for regional CO_2 flux inversion using a Lagrangian Particle Dispersion Model (LPDM) driven by the output of SiB-RAMS. The method involves four steps: (1) forward simulation of photosynthesis, respiration, decomposition, and atmospheric transport using the coupled SiB-RAMS model; (2) calculation of a large number of backward-in-time particle trajectories from each observation point ("receptor") in space and time; (3) integration of the particle trajectories to quantify the "influence function" of each upstream grid cell at each previous time with respect to a particular observation; and (4) an optimization scheme that adjusts the fluxes so that simulated and observed mixing ratios differ by acceptable amounts. This method was developed partly with prior support from DOE TCP, and was tested using data from the Ring of Towers experiment (see results from prior TCP research described previously). The LPDM (Uliasz and Pielke, 1991; Uliasz, 1993, 1994; Uliasz et al., 1996) accounts for transport by resolved advection and by subgrid-scale stochastic motion (turbulence and clouds). Influence functions calculated by integrating upstream contact time with the surface quantify the partial derivative of a particular measurement with respect to all previous fluxes at all surface points in the domain (the method is nearly identical to that of Gerbig et al., 2003b). In general, influence functions are also calculated with respect to the initial distribution of CO_2 and the lateral boundary conditions, though with sufficient integration time the former become negligible.

We account for high-frequency time variations of photosynthesis and respiration by assuming that they are driven by well-understood and easily modeled processes (radiation, temperature, soil moisture), then solve for unknown multiplicative biases in each component flux after smoothing in space and time. This is accomplished by convolving the influence functions generated from LPDM with gridded photosynthesis (gross primary production, GPP) and ecosystem respiration (RESP) at each time step in SiB-RAMS. The net ecosystem exchange (NEE) is composed of these two component fluxes:

$$NEE(x,y,t) = RESP(x,y,t) - GPP(x,y,t) \qquad \text{(eq 1)}$$

where x and y represent grid coordinates and t represents time. Sub-hourly variations in the simulated component fluxes in time are primarily controlled by the weather (especially changes in radiation due to clouds and the diurnal cycle of solar forcing), whereas seasonal changes are derived from phenological calculations parameterized from satellite imagery. Fine-scale variations in space are driven by variations in vegetation cover, soil texture, and soil moisture. To estimate regional fluxes from atmospheric mixing ratios, we assume that the model of the component fluxes is biased, and that the biases are smoother in time and space than the fluxes themselves:

$$NEE(x,y,t) = \beta_{RESP}(x,y)RESP(x,y,t) - \beta_{GPP}(x,y)GPP(x,y,t) \qquad \text{(eq 2)}$$

A persistent bias in photosynthesis might result from underestimation of leaf area, available nitrogen, or soil moisture, whereas a persistent bias in respiration might result from overestimation of soil carbon or coarse woody debris. In any case, it is reasonable that such biases vary much more slowly than the fluxes themselves.

To estimate slowly-varying biases β_{Resp} and β_{GPP} using SiB-RAMS and LPDM, we first generate surface flux influence functions by integrating the backward-in-time particle trajectories from LPDM. Using these, we can represent the mixing ratio observed at a given station k at time m as

$$C_{k,m} = \sum_{i,j,n}\left(\left(\beta_{R,i,j}RESP_{i,j,n} - \beta_{A,i,j}GPP_{i,j,n}\right)C^{*}_{k,m,i,j,n}\right)\Delta t_f \Delta x \Delta y + C_{BKGD,k,m} \qquad \text{(eq 3)}$$

where i and j are grid indices in the zonal and meridional directions, n is the time at which GPP and Respiration occurred (not usually the time at which the resulting change in mixing ratio was measured!). The influence function $C^{*}_{k,m,i,j,n}$ is then the discrete form of the partial derivative of the observed mixing ratio with respect to the NEE at grid cell (i,j) at time step n. The length scales Dx and Dy are the sizes of the grid cells in the zonal and meridional direction, and Dt_f is the time step over which the fluxes are applied. The term $C_{BKGD,k,m}$ represents the contribution of "background" CO_2 flowing into the model domain from the larger scales. With a little algebra and a healthy dose of computer time, we obtain a simpler representation more practical suitable for optimization:

$$C_{obs} = \sum_{cell=1}^{nCell}\beta_{RESP,cell}C^{*}_{RESP,obs,cell} + \sum_{cell=1}^{nCell}\beta_{GPP,cell}C^{*}_{GPP,obs,cell} + C_{BKGD,obs} \qquad \text{(eq 4)}$$

where obs is an observation number (combines indices k and m), and $cell$ is a grid cell number (combines indices i and j). The influence functions have been convolved with the GPP and RESP terms from the forward model and integrated over the time period over which the bias terms are assumed to apply:

$$\begin{aligned} C^{*}_{RESP,obs,cell} &= \Delta t_f \Delta x \Delta y \sum_n RESP_{cell,n}C^{*}_{obs,cell,n} \\ C^{*}_{GPP,obs,cell} &= -\Delta t_f \Delta x \Delta y \sum_n GPP_{cell,n}C^{*}_{obs,cell,n} \end{aligned} \qquad \text{(eq 5)}$$

We have experimented successfully with 10-day time scales for the bias terms, which allow influence functions on hourly fluxes and observations to be integrated for 240 hours. This approach has two important advantages: (1) the area and strength of upstream influence over 10 days is much greater than for a single hour, so the inverse problem of estimating the bias terms β is much better constrained than the estimation of the fluxes themselves; and (2) the storage of the influence functions in (eq 5) is 240 times smaller than would be required to store all the $C_{obs,cell,n}$!

Equation 4 is a linear system which can be written simply as

$$\vec{y} = h\vec{x} \qquad \text{(eq 6)}$$

where $\vec{y}$ is the vector of observations C_{obs} and $\vec{x}$ is the vector of unknown bias terms $\beta_{\mathrm{GPP,cell}}$ and $\beta_{\mathrm{Resp,cell}}$. The Jacobian matrix h contains the influence functions $C^{*}_{GPP,obs,cell}$ and $C^{*}_{RESP,obs,cell}$. The rows of h correspond to each observation, and each column corresponds to an unknown bias term β_{RESP} or β_{GPP} at a given grid cell over the 10-day integration period. In practice, we treat the background mixing ratio by prescribing lateral inflow from a larger scale model. We treat errors in this boundary condition additively by augmenting the vector of unknowns $\vec{x}$ with lateral boundary concentrations and "transporting" them to the receptor by augmenting matrix h with additional influence functions for these fluxes.

5.2.3 Estimation of Bias Terms from Atmospheric Mixing Ratios with MLEF

For relatively small numbers of unknowns and observation, the inverse problem of estimating $\vec{x}$ from $\vec{y}$ in (eq 6) is straightforward and can be solved by matrix methods involving singular-value decomposition (SVD). We minimize a cost function that penalizes model-data mismatch and is regularized by imposing a weak prior constraint:

$$J = (\vec{y} - h\vec{x})^T r^{-1}(\vec{y} - h\vec{x}) + (\vec{x} - \vec{x}_p)^T p^{-1}(\vec{x} - \vec{x}_p)$$

here r is the observation error covariance, and p is the prior error covariance of the unknown β's. The solution is given (e.g., Rodgers, 2000) by

$$\vec{x} = \vec{x}_p + (h^T r^{-1} h + p^{-1})^{-1} h^T r^{-1} (\vec{y} - h\vec{x}_p) \qquad \text{(eq 7)}$$

and the *a posteriori* error covariance of the b's is given by

$$c = (h^T r^{-1} h + p^{-1})^{-1}. \qquad \text{(eq 8)}$$

To solve (eqs 7 and 8), we use a fast and flexible algorithm for this "analytical" inversion, originally derived by Peter Rayner (pers. comm.), and implemented in the IDL programming language. Continental inversions of hourly data from 11 towers for 10-day biases in GPP and RESP on a 100-km grid with (4408 unknowns with 2640 observations) take about 10 minutes of CPU time using this routine on a fast Linux machine. Unfortunately, the computing requirements for the analytical solution to the inverse problem scale roughly as the square of the number of unknowns or observations, and large problems will not fit in computer memory. This method is also limited to linear models with (assumed) Gaussian errors. To overcome these obstacles and for more flexibility with respect to optimizing structures in the error covariance in the bias terms β, we have implemented the model described above into the Maximum Likelihood Ensemble Filter (Zupanski, 2005; Fletcher and Zupanski, 2006), which is closely related to the Ensemble Kalman Filter (Peters et al, 2005). The MLEF is very flexible, allowing for nonlinear models of arbitrary complexity and for non-Gaussian errors. It has been adapted for separate estimation of model error as well as optimal control parameters. The essence of the ensemble data assimilation approach is that an ensemble of sets of systematically perturbed control parameters (the β's in our case) are generated by the algorithm from an initial forward simulation and calculation of model-data mismatch ($\vec{y} - h\vec{x}$ in our case). An ensemble of forward model integrations (for us, the simple matrix multiplication $h\vec{x}$) is then performed, and the optimization algorithm estimates values and uncertainties of each control parameter from the resulting dependence of model-data mismatch on parameter values, subject to specified prior values and error covariance.

The ensemble yields an approximation of the full error covariance matrix of the β's, the accuracy of which depends on the size of the ensemble. Theoretically, the MLEF estimation approaches the analytical solution (eqs 7 and 8) when the size of the ensemble is equal to the number of unknowns (this is called the "full-rank" problem). We have verified this behavior for continental and regional inversions of SiB-RAMS fluxes by comparing estimates of β (x,y) and its error covariance computed with full-rank ensembles to the analytical solution. The MLEF algorithm includes a strong preconditioning step that reduces the size of ensembles required. In our experiments with estimation of SiB-RAMS biases for the Ring of Towers, we have found that ensembles of 100 members produce results that are almost indistinguishable from the full-rank solution (1800 members).

A key advantage of the estimation of β (x,y) using the MLEF is that spatial covariance and correlation between biases in GPP and respiration can be propagated from one 10-day "assimilation cycle" to the next, so that spatial patterns in the bias emerge over time. In any given time window, the model is terribly underconstrained by observations, but the system "learns" about the model biases and their spatial structure over successive cycles as new observations are assimilated. Without spatial patterns of error covariance, inverse methods are prone to creating unrealistic flux patterns determined by the placement of the observations. Alternatively, one can assume that model biases are determined uniquely by vegetation type (Gerbig et al, 2003b, 2005), but this risks extreme aggregation error. Biases due to incorrect soil nitrogen or forest stand age, for example, are very unlikely to be constant across all pixels of a given vegetation type.

Regional Evaluation of SiB-RAMS-LPDM-MLEF for the Ring of Towers

We have evaluated the ability of the MLEF to estimate biases in SiB-RAMS fluxes given influence functions generated by the LPDM using synthetic observations for the Ring of Towers experiment in the summer of 2004. A forward simulation of a 70-day period starting on 1 June, 2004 was performed in SiB-RAMS on a domain somewhat larger than the conterminous USA on a grid of Dx=40 km. A finer nest was run on a 1000 km x 1000 km subdomain centered on WLEF with Dx =10 km. Influence functions were generated by running the LPDM backward in time for two-hour mean "samples" from six surface layer towers in the Ring, plus five levels on the WLEF tower (all but the 11 m level). We then sought to estimate the bias factors every 10 days (seven assimilation cycles) on a 20-km grid over a 600 x 600 km area centered on the tall tower.

We created a "true" field of the biases in SiB-RAMS simulations of GPP and ecosystem respiration (β_{RESP} and β_{GPP}) by dividing the domain in half. On the east side, we set the mean value of both β's to be 1.1, and on the western half we set them to 0.5. To make the problem more difficult, we also included random deviations in each β chosen from a Gaussian distribution with a mean of 0 and a standard deviation of 0.1. Because we are gluttons for punishment, we applied these deviations with different decorrelation length scales: 80 km in the southern and 160 km in the northern halves of the domain. We then used these perturbed β's to generate synthetic mixing ratio data by multiplying them by the LPDM influence functions (eq 6), which were already convolved with the modeled photosynthesis and respiration from SiB-RAMS, as two-hourly averages assuming that the model bias is constant over periods of 10-days. The data were also perturbed by Gaussian noise, with a mean of 0 and a variance that depended on tower height and time of day. The error assigned to the data ranged from 1 ppm above 200 m during daytime to 45 ppm below 50 m at night. Note that this formulation only allows about three "observations" per day from the surface-layer towers under well-mixed conditions, and very strongly deweights night-time and transitional values.
As a "first guess" of the unknown distribution of model bias, we assumed a uniform field of β = 0.75 in every grid cell. This value was assumed to be known to within 0.2 (at 1-sigma). Our initial estimate of the spatial decorrelation length-scale was 120 km. Successive cycles in the assimilation used the estimated β's and covariance matrix from the previous cycle as a background field, constituting a "persistence forecast" for both the β's and their covariance structure. No further smoothing was applied. After the first cycle, the spatial covariance of the errors in β's was determined from the synthetic mixing ratio data. Results (Fig 3) are very encouraging. The estimated β (x,y) clearly distinguish the east-west structure in the "true" field, and also capture much of the random finer variations, including the smoother patterns in the south than the north. The constraint is weak over the Great Lakes, because both GPP and Resp are zero there. Overall uncertainty in the model bias was less than 5% over most of the interior of the Ring.

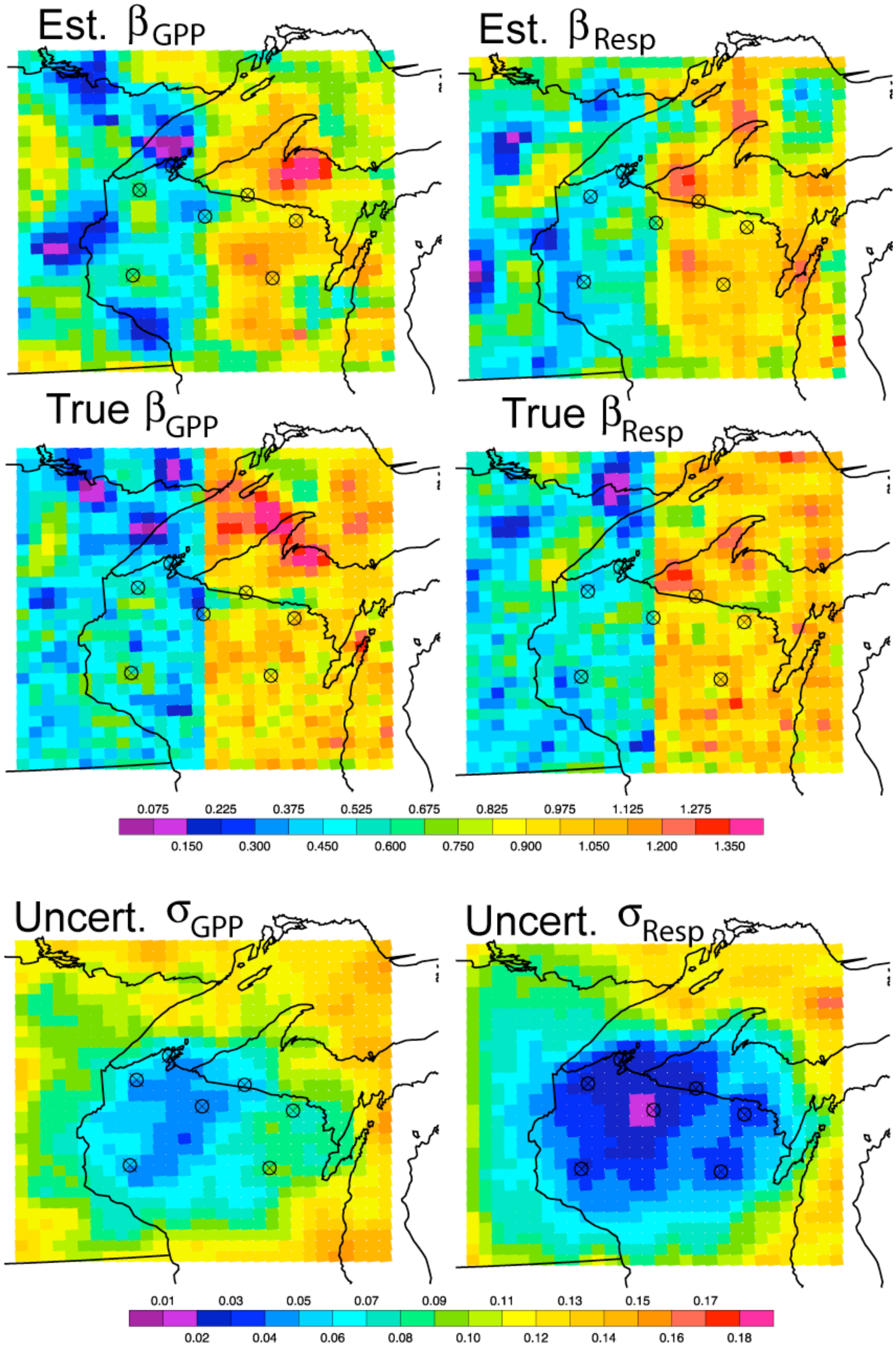
Est. β_{GPP}
Est. β_{Resp}
True β_{GPP}
True β_{Resp}
0.075 0.225 0.375 0.525 0.675 0.825 0.975 1.125 1.275
0.150 0.300 0.450 0.600 0.750 0.900 1.050 1.200 1.350
Uncert. σ_{GPP}
Uncert. σ_{Resp}
0.01 0.03 0.05 0.07 0.09 0.11 0.13 0.15 0.17
0.02 0.04 0.06 0.08 0.10 0.12 0.14 0.16 0.18

References

Baker, I., A.S. Denning, N. Hanan, L. Prihodko, M. Uliasz, P.-L. Vidale, K.J. Davis, and P.S. Bakwin, 2003. Simulated and Observed Fluxes of Sensible and Latent Heat and CO2 at the WLEF-TV Tower Using SiB2.5. *Global Change Biology*, **9**, 1262-1277.

Bakwin, P.S., Tans, P.P., Hurst, D.F., and Zhao, C., 1998. Measurements of carbon dioxide on very tall towers: Results of the NOAA/CMDL program, Tellus, 50B, 401–415.

Baldocchi, D., Falge, E., Gu, L., Olson, R., Hollinger, D., Running, S., Anthoni, P., Bernhofer, Ch., Davis, K., Evans, R., Fuentes, J., Goldstein, A., Katul, G., Law, B., Lee, X., Malhi, Y., Meyers, T., Munger, W., Oechel, W., Paw U, K. T., Pilegaard, K., Schmid, H. P., Valentini, R., Verma, S., Vesala, T., Wilson, K., and Wofsy, S., 2001. FLUXNET: A new tool to study the temporal and spatial variability of ecosystem- scale carbon dioxide, water vapor, and energy flux densities, Bull. Amer. Meteor. Soc., 82, 2415–2434.

Bresee, M.K., Le Moine, J., Mather, S., Brosofske, K.D., Chen, J., Crow, T.R., and Rademacher, J., 2004. Disturbance and landscape dynamics in the Chequamegon National Forest, Wisconsin, USA, from 1972 to 2001, Land. Ecol., 19 (1), 291–309.

Bousquet, P., Peylin, P., Ciais, P., LeQuere, C., Friedlingstein, P., and Tans, P., 2000. Regional changes in carbon dioxide fluxes of land and oceans since 1980, Science, 290, 1342–1346.

Chan, D., Yuen, C.W., Higuchi, K., Shashkov, A., Liu, J., Chen, J., and Worthy, D., 2004. On the CO2 exchange between the atmosphere and the biosphere: the role of synoptic and mesoscale processes, Tellus, 56B, 194–212.

Cook, B.D., Davis, K.J., Wang, W., Desai, A.R., Berger, B.W., Teclaw, R.M., Martin, J.M., Bolstad, P., Bakwin, P., Yi, C., and Heilman, D., 2004. Carbon exchange and venting anomalies in an upland
deciduous forest in northern Wisconsin, USA, Agric. Forest Meteor., 126 (3–4), 271–295.

Davis, K.J., Bakwin, P.S., Yi, C., Berger, B.W., Zhao, C., Teclaw, R.M., and Isebrands, J.G., 2003. The annual cycles of CO2 and H20 exchange over a northern mixed forest as observed from a very tall tower, Global Change Biol., 9 (9), 1278–1293.

Denning, A.S. et al., *Science Implementation Strategy for the North American Carbon Program.* **http://www.carboncyclescience.gov**, 2005.

Denning, A. S., Collatz, J. G., Zhang, C., Randall, D. A., Berry, J. A., Sellers, P. J., Colello, G. D., and
Dazlich, D. A., 1996a. Simulations of terrestrial carbon metabolism and atmospheric CO2 in a general circulation model, Part 1: Surface carbon fluxes, Tellus, 48B, 521–542.

Denning, A. S., Randall, D. A., Collatz, G. J., and Sellers, P. J., 1996b. Simulations of terrestrial carbon metabolism and atmospheric CO2 in a general circulation model, Part 2: Spatial and temporal variations of atmospheric CO2, Tellus, 48B, 543–567.

Desai, A., A. Noormets, P. V. Bolstad, J. Chen, B. D. Cook, K. J. Davis, E. S. Euskirchen, C. Gough, J. M. Martin, D. M. Ricciuto, H. P. Schmid, J. Tang, and W. Wang, In press a. Influence of vegetation type, stand age and climate on carbon dioxide fluxes across the Upper Midwest, USA: Implications for regional scaling of carbon flux. In press, *Agricultural and Forest Meteorology*.

Desai, A.R., P.R. Moorcroft, P.V. Bolstad and K.J. Davis, In press b. Regional carbon fluxes from a
observationally constrained dynamic ecosystem model: Impacts of disturbance, CO_2 fertilization, and
heterogeneous land cover. In press, *J. Geophysical Research Biogeosciences.*

Enting, I. G., Trudinger, C. M., and Francey, R. J., 1995. A synthesis inversion of the concentration and delta 13C of atmospheric CO_2 , Tellus, 47B, 35–52.

Fan, S., Gloor, M., Mahlman, J., Pacala, S., Sarmiento, J., Takahashi, T., and Tans, P., 1998. A large
terrestrial carbon sink in North America implied by atmospheric and oceanic carbon dioxide data and
models, Science, 282, 442–446.

Gerbig, C., J.C. Lin, S.C. Wofsy, B.C. Daube, A.E. Andrews, B.B. Stephens, P.S. Bakwin, and C.A.
Grainger, 2003. Toward constraining regional-scale fluxes of CO_2 with atmospheric observations over a continent: 2. Analysis of COBRA data using a receptor-oriented framework, *Journal of Geophysical Research D: Atmospheres*, **108** (D24, 4757), (doi:10.1029/2003JD003770).

Gloor, M., Fan, S.M., Pacala, S., Sarmiento, J., 2000. Optimal sampling of the atmosphere for purpose of inverse modeling: A model study, Global Bio. Cycles, 14(1), 407–428.

Goulden, M. L., Wofsy, S. C., Harden, J. W., Trumbore, S. E., Crill, P. M., Gower, S. T., Fries, T., Daube, B. C., Fan, S.-M., Sutton, D. J., Bazzaz, A., and Munger, J. W., 1998. Sensitivity of boreal forest carbon balance to soil thaw, Science, 279, 214–218.

Gurney, K.R., Law, R.M., Denning, A.S., Rayner, P.J., Baker, D., Bousquet, P., Bruhwiler, L., Chen, Y.-H., Ciais, P., Fan, S., Fung, I.Y., Gloor, M., Heimann, M., Higuchi, K., John, J., Maki, T., Maksyutov, S., Masarie, K., Peylin, P., Prather, M., Pak, B.C., Randerson, J., Sarmiento, J., Taguchi, S., Takahashi T., and Yuen, C.-W., 2002. Towards robust regional estimates of CO_2 using atmospheric transport models, Nature, 415, 626–630.

Hurwitz, M.D., Ricciuto, D.M., Bakwin, P.S., Davis, K.J., Wang, W., Yi, C., and Butler, M.P., 2004.
Transport of carbon dioxide in the presence of storm systems over a northern Wisconsin forest, J. Atmos. Sci., 61, 607–618.

Janssens, I.A., G.-J. Nabuurs, G. Folberth, B. Schlamadinger, R.W.A. Hutjes, R. Ceulemans, E.-D. Schulze, R. Valentini, A.J. Dolman, A. Feibauer, P. Ciais and P. Smith, 2003. Europe's terrestrial biosphere absorbs 7 to 12% of European anthropogenic CO_2 emissions. *Science,* **300**, 1538-1542.

Kitzis, D., and Zhao, C., 1999. CMDL/Carbon Cycle Greenhouse Gases Group standards preparation and stability. NOAA Tech. Memo ERL-14, 14 pp.

Law, R.M., Rayner, P.J, Steele, L.P., Enting, I.G., 2002. Using high frequency data for CO_2 inversions, Global Bio. Cycles, 16(4), 1053, doi:10.1029/2001G001593.

Mackay, D.S., B.E. Ewers, B,D. Cook, and K.J. Davis, Environmental drivers of evapotranspiration in a shrub wetland and an upland forest in northern Wisconsin. In press, Water Resources Research.

Masarie, K. A. and Tans, P. P., 1995. Extension and integration of atmospheric carbon dioxide data into a globally consistent measurement record, J. Geophys. Res., 100(D6), 11593–11610.

Masarie, K. A., Langenfelds, R. L., Allison, C. E., Conway, T. J., Dlugokenchy, E. J., Francey, R. J.,
Novelli, P. C., Steele, L. P., Tans, P. P., Vaughn, B., and White, J. W. C., 2001. NOAA/CSIRO Flask Air Intercomparison Experiment: A strategy for directly assessing consistency among atmospheric
measurements made by independent laboratories, J. Geophys. Res., 106(D17), 20445–20464.

Matross, D.M., J.C. Lin, S.C. Wofsy, B.C. Daube, E.W. Gottlieb, V.Y. Chow, J.T. Lee, C. Zhao, P.S. Bakwin, J.W. Munger, D.Y. Hollinger, A. Andrews, M. Pathmathevan and C. Gerbig, 2006. Estimating regional carbon exchange in New England and Quebec by combining atmospheric, ground-based and satellite data. *Tellus B*, **58**, 344-358.
NCEP, 2004. [Available from National Climatic Data Center, Federal Building, 151 Patton Avenue,
Asheville, NC 28801-5001.]

NOAA, 2004. [Available from Climate Monitoring and Diagnostics Laboratory, 325 Broadway R/CMDL 1, Boulder, CO 80305-3328.]

Pacala, S.W., Hurtt, G.C., Houghton, R.A., Birdsey, R.A., Heath, L., Sundquist, E.T., Stallard, R.F. Baker, D., Peylin, P., Ciais, P., Moorcroft, P., Caspersen, J., Shevliakova, E., Moore, B., Kohlmaier, G., Holland, E., Gloor, M., Harmon, M.E., Fan, S.-M., Sarmiento, J.L., Goodale, C., Schimel, D., and Field, C.B., 2001. Convergence of land- and atmosphere based U.S. carbon sink estimates, Science, 292, 2316–2320.

Rayner, P. J., Enting, I. G., and Trudinger, C. M., 1996. Optimizing the CO2 observing network for
constraining sources and sinks. Tellus, 48B, 433–444.

Rayner, P. J., I. G. Enting, R. J. Francey, and R. Langenfelds, 1999. Reconstructing the recent carbon cycle from atmospheric CO2, δ13C, and O2/N2 observations, Tellus, 51B, 213–232.

Ricciuto, D. M., M. P. Butler, K. J. Davis, B. D. Cook, P. S. Bakwin, A. E. Andrews, and R. M. Teclaw. Causes of interannual variability in ecosystem-atmosphere CO2 exchange in a northern Wisconsin forest using a Bayesian synthesis inversion. In press, *Agricultural and Forest Meteorology*.

Wang, J.-W., A. S. Denning, L. Lu, I. T. Baker, K. D. Corbin, K. J. Davis, Observations and simulations of synoptic, regional, and local variations in atmospheric CO2. In press, *J. Geophys. Res. Atmos*.

Wang, W., K.J. Davis, B.D. Cook, M.P. Butler, and D.M. Ricciuto, 2006. Decomposing CO2 fluxes measured over a mixed ecosystem at a tall tower and extending to a region: A case study. *J. Geophys. Res. Biogeosci.* **111** (G02005), doi:10.1029/2005JG000093

Wofsy, S. C., Goulden, M. L., and Munger, J. W., 1993. Net exchange of CO2 in a mid-latitude forest, Science, 260, 1314–1317.

Zhao, C.L., Tans, P., and Thoning, K.W., 1997. A high precision manometric system for absolute calibrations of CO2 in dry air, J. Geophys. Res., 102(D5), 5885–5894.